Structural and electronic properties of ion-beam-prepared $Al_{1-x}Fe_x$ samples

Structural and electronic properties of ion-beam-prepared Al$_{1-x}$Fe$_x$ samples

Agnès Traverse†+, Esther Belin-Ferré‡, Zoltán Dankházi§,
Luis Mendoza-Zélis‖, Olivier Laborde¶ and Richard Portier††

† Laboratoire pour l'Utilisation du Rayonnement Electromagnétique, Bâtiment 209A, Université Paris-Sud, 91405 Orsay Cédex, France
‡ LCPMR (Unité de Recherche associeé au CNRS 176), 11 rue P et M Curie, 75231 Paris Cédex 05, France
§ Institute for Solid State Physics, Eötvös University, Múzeum krt. 6-8, 1088 Budapest, Hungary
‖ Departamento de Fisica, Universidad Nacional de La Plata, CC 67, 1900 La Plata, Argentina
¶ CRTBT CNRS, BP 166 X, 38042 Grenoble Cédex, France
†† Ecole Nationale Supérieure de Chimie de Paris, Laboratoire de Métallurgie Structurale, 11 rue Pierre et Marie Curie, 75005 Paris, France

Abstract. Al$_{1-x}$Fe$_x$ thin films, with $x = 0.14$ and 0.23, were prepared from alternate Al and Fe layers by irradiation with a Xe beam at two different temperatures in order to reach either the amorphous or the quasicrystalline state. Through thermal treatment, crystalline alloys are obtained. Rutherford back-scattering spectrometry of α-particles and transmission electron microscopy have been used to characterize the atomic distribution and structural state of the samples. X-ray emission spectroscopy and conversion electron Mössbauer spectroscopy provided information about the electronic distributions whereas electrical resistivity measurements allowed us to determine the metallic character of the compounds. The existence of a pseudo-gap and dehybridization of the s and d electronic states of Fe are suggested to interpret the high-resistivity behaviour and the isomer shift values, measured in the Fe concentration range studied here.

1. Introduction

Alloys of aluminium and transition metal (TM) are interesting systems from both structural and electronic points of view. It has been shown for the first time by Shechtman *et al* (1984) that, in addition to the well crystallized and amorphous states, Al and Mn can form, in certain preparation conditions, a quasicrystalline (QC) atomic arrangement for Al concentrations of about 80%. Then it appeared that other Al-TM alloys display the same structural QC state. (Tsai *et al* 1988). High values of electrical resistivity were measured in several Al–TM alloys that were correlated to the existence of a pseudo-gap at the Fermi level (Belin and Traverse 1991, Berger *et al* 1993). Up to now, ternary systems such as Al–Cu–Fe, Al–Pd–Mn and Al–Pd–Re have been extensively studied since they can have very good structural quality (absence of atomic disorder) together with very high resistivity values at low temperatures of the order of a few thousands of microhm centimetres up to a few ohm centimetres (Pierce *et al* 1993, and Poon *et al* 1995).

To our knowledge, only a few binary alloys have been synthesized and studied so far. Among the techniques suitable for preparing binary Al–TM alloys in several structural

---

+ Author to whom correspondence should be addressed. E-mail: TRAVERSE@lure.u-psud.fr.

states, ion beam techniques seemed to be useful because of the capability of attaining single-phase systems. Depending on the sample temperature during the treatment, amorphous (A), QC or even crystalline (C) topological arrangements can be formed (Alexandre *et al* 1992, Baumvol 1992).

In this work, we have chosen to study the $Al_{1-x}Fe_x$ system which can be considered as a starting point for understanding the Al–Cu–Fe system. It was prepared from alternate Al and Fe layers irradiated with a Xe beam at two different temperatures in order to get either the A or the QC state. A few samples were then thermally heated to obtain a C state. The goal was to correlate the three structural states to the electronic properties for two different Fe concentrations.

Several workers have already performed Al–Fe mixing, usually with Xe ions of energy $E > 500$ keV, which are the most efficient (Karpe *et al* 1992, Plenet *et al* 1993, Brenier *et al* 1994). Baumvol (1992) also tried Ar at 100 keV. The Fe concentrations used were 0.18 by Plenet *et al* (1993) and Hohmuth *et al* (1989), 0.17, 0.20 and 0.35 by Karpe *et al* (1992) and 0.25 by Baumvol (1992). The concentrations that we have chosen for our samples are either lower ($x = 0.14$) which allows us to extend the Fe concentration range already studied, or in between ($x = 0.23$) to compare our results with those already published. We emphasize that, to our knowledge, a study where, for a given Fe concentration, the three structural states are compared from the point of view of the electronic properties had never been carried out. As Fe is a good Mössbauer probe, we must mention the exhaustive study via the Mössbauer effect of $Al_{1-x}Fe_x$ for $x = 0$ to 1 performed by Hsu and Chien (1991). The alloys prepared by sputtering were A in the range 0.15–0.45 and BCC random solid solutions in the range 0.45–1. The Mössbauer effect was also investigated in Fe-implanted Al with concentrations from 0.02 to about 0.4 (Sawicka *et al* 1978).

To correlate electronic properties and structural states, we have combined several experimental techniques. Rutherford back-scattering spectrometry (RBS) of α-particles was used to determine the Al and Fe in-depth concentrations before and during the ion beam mixing. The A or QC structural states were characterized using transmission electron microscopy (TEM) measurements. X-ray emission spectroscopy (XES) allowed us to investigate the electronic distributions of occupied states. In addition, conversion electron Mössbauer spectroscopy (CEMS) provided information on the short-range atomic order and the local electronic densities at the Fe sites via the quadrupole splitting (QS) and isomer shift (IS) values. Finally electrical resistivity measurements were performed since resistivity is a good indication of the 'metallic' or 'non-metallic' character of a system.

The paper is organized as follows. The experimental procedures are summarized in section 2, the results are described in section 3 and are then discussed in section 4.

2. Experimental techniques

2.1. Sample preparation and characterization

The Al/Fe stacks were prepared by electron gun evaporation of the elemental constituents on quartz substrates at a base pressure of 1.3×10^{-8} mbar. Prior to evaporation, iron was ^{57}Fe enriched in order to enhance the Mössbauer absorption. Four series of multilayers consisting of six Al/Fe bilayers were prepared; details are given in table 1. Additionally 3.0 nm of Al were deposited on top of each multilayer as a barrier to oxygen penetration. The stacks were irradiated with Xe^{3+} at 570 keV up to a fluence of $(2.5–3.0)\times10^{15}$ cm^{-2}. This incident energy was chosen so that, following a calculation with the TRIM code (Ziegler *et al* 1986), the Xe ions go through the whole Al/Fe stack and deposit a large part of their incoming

energy in the form of atomic collisions (3 keV nm^{-1}), which is efficient to mix the layers. Irradiations were performed for substrate temperatures of 20 and 190 °C. The choice of the total fluence was guided by several arguments as explained later.

Table 1. List of the samples with their treatments (substrate temperature and Xe fluence used for mixing and post-annealing temperatures), the structural state (A, amorphous; QC, quasicrystalline; C, crystalline) after irradiation and average concentrations together with the concentration inhomogeneities as detected from RBS (see text).

Sample	Layered structure	Irradiating fluence (10^{15} cm^{-2})	Irradiation temperature (°C)	Annealing temperature (°C)	Average composition	Structural state
a	6(14.8Al + 2.3Fe) nm	2.5	20	200, 350	Al$_{0.77}$Fe$_{0.23}$	A
				500	($x = 0.23 \pm 0.012$)	C
b	6(14.8Al + 2.3Fe) nm	2.5	190	200	Al$_{0.77}$Fe$_{0.23}$	QC
				350	($x = 0.23 \pm 0.006$)	
				500		C
c	6(21.7Al + 2.8Fe) nm	3	20	200	Al$_{0.86}$Fe$_{0.14}$	A
d	6(21.7Al + 2.8Fe) nm	3	190	350	Al$_{0.86}$Fe$_{0.14}$	QC
					($x = 0.14 \pm 0.022$)	

Various stacks made of Al and natural Fe were evaporated onto cleaved NaCl, in order to remove them easily from the substrate and to deposit them on Cu grids. They were irradiated in the same conditions as described above and used for characterization of the structural state owing to TEM measurements.

Heat treatments were performed either in a heating device continuously evacuated by a turbomolecular pump at a pressure lower than 2×10^{-5} mbar or in a conventional oven in evacuated quartz ampoules (p< 2×10^{-5} mbar).

The in-depth composition of the multilayers deposited on quartz, before and during irradiation or after heat treatment, was analysed by RBS of α-particles using the ARAMIS facility (Bernas *et al* 1992). An incident beam of 1.2 MeV He$^+$ particles was sent and the back-scattered particles were detected at 175° with a Si detector whose resolution is 10 keV. The energy of the back-scattered particles depends firstly on the target atom on which the collision has taken place and secondly on the depth at which the back-scattering process has occurred. The fitting of the Rutherford back-scattering spectra which consist in the number of back-scattered particles versus their energy provides quantitative information on the nature of atoms in the target and their in-depth distribution. Hence it is possible to follow during the irradiation the evolution of the layered structure and in particular to detect the fluence for which the mixing is achieved. The maximum irradiating fluence was then chosen when the layered structure had totally disappeared in the Rutherford back-scattering spectra and when the TEM observations confirmed the absence of remaining pure Al or Fe phase. Note that, Baumvol (1992) and Alexandre *et al* (1992) also used a fluence of 5×10^{15} Xe cm^{-2}, of the same order of magnitude as in this work, for a slightly lower Xe energy (300 keV instead of 570 keV).

As the Fe signal is well separated from the signal due to Al atoms located in the stack or Si and O atoms located in the substrate, it is possible to deduce the total number of Fe atoms in the samples by comparing the signal area with that of a standard specimen. These values represent thus a constraint in the fitting procedure done with the RUMP code

(Doolittle 1986) and are important especially to deduce the relative atomic concentration.

2.2. Mössbauer spectroscopy

Mössbauer spectroscopy allows one to observe transitions between non-excited and excited nuclear states of a solid owing to the resonant absorption of γ photons. This technique is particularly well adapted to the study of alloys with Fe atoms since ^{57}Fe is the best Mössbauer isotope. It gives information about the energy separation between these nuclear states. These are distinctly affected by the electronic environment, through the IS value which is sensitive to the s-like electronic density at the probe nucleus. CEMS also gives information on the splitting of these levels produced by extranuclear fields. The QS values measure the quadrupole coupling between the probed nuclear moment and the electric field gradient produced by the charge distribution around them.

Conversion electron Mössbauer spectra were obtained in the constant-acceleration mode using the ^{57}Co–Rh source and an electron counter with a steady flow of He–8 at.% CH$_4$. All measurements were performed at room temperature.

In general the spectra were fitted alternatively with

(i) a single asymmetric doublet of broadened Lorentzians,
(ii) two symmetric doublets of broadened Lorentzians and
(iii) a distribution of quadrupole doublets (QSD) with a linear correlation between the IS and the QS: IS $=$ IS$_0 + \alpha$ QS.

2.3. Soft x-ray and photoemission spectroscopies

The XES investigates separately occupied band (OB) states of all the components of a solid owing to transitions that involve an inner level $\mathcal{L}$ of one of the constituents of the solid and states of the OB. Because the x-ray transitions are governed by dipole selection rules, s, p or d states are studied independently and, because the inner hole is on a given atomic site, the information is also site related. The intensities emitted during an XES process are proportional to $|M|^2 \mathcal{N}_{occ}(\epsilon) \cdot \mathcal{L}_{n,\ell}$. M is the matrix element of the transition probability; it depends upon the overlap between the initial and final wavefunctions of the system; it is usually considered as being constant over the energy ranges which are investigated here or varies slowly against energy. $\mathcal{N}_{occ}(\epsilon)$ is the OB density of states DOS probed during the measurement. $\mathcal{L}_{n,\ell}$ is the Lorentzian-like energy distribution of the inner level involved in the x-ray transition. Thus, the shapes of the x-ray spectral curves are directly connected to the DOS broadened by the Lorentzian-like energy distribution of the inner level and multiplied by M. Therefore, no absolute DOS values can be obtained. However, it is possible to compare curves of a given spectral character for a given element in various solids. On the other hand, in the x-ray photoelectron spectroscopy (XPS) technique, incident radiation transfers its energy to electrons that are thus ejected from the solid. This technique makes it possible to measure separately the kinetic energies of the ejected electrons and consequently their binding energy in the solid provided that suitable energy calibration is done to account for the work function. XPS allows us, in particular, to obtain the binding energies of the core levels involved in x-ray transitions. Thus it is feasible to place the Fermi level energy on the various x-ray transition energy scales, and so adjustment of the partial local electronic distributions in the binding energy scale is possible. Consequently, insight is gained into the interactions between the various electronic distributions in a solid.

Al 3p and Fe 3d–4s OB states were probed owing to the measurement of the x-ray transitions Al Kβ (OB $\rightarrow$ Al 1s) and Fe Lα (OB $\rightarrow$ Fe 2p$_{3/2}$). Note that in this latter

case, due to the transition probabilities, Fe 3d states are essentially investigated. The corresponding energy ranges are about 1560 eV and 710 eV, i.e. the energy range of soft x-rays that may be analysed using crystals.

The Al–Fe thin films deposited onto convenient holders were water cooled and used as the targets of the x-ray tube; they were irradiated with incoming electrons or photons so that, in both cases, the whole thickness of the sample contributes to the x-ray emission. The measurements were carried out in Johann-type vacuum spectrometers equipped with electronic detection and fitted with a bent 1010 quartz plate used in the first reflection order for investigating Al spectra or a RbAP slice used in the second reflection order for the Fe spectra. The spectral resolutions are 0.3 eV and 0.5 eV, respectively, for Al and Fe (table 2).

Table 2. From left to right, in the first four columns are reported the names of the x-ray lines, the x-ray transitions and energy ranges investigated. The last column gives the distance parameters and energy resolution of the crystals used to analyse the x-ray transitions.

X-ray line	Transition	Investigated states	Energy range (eV)	Crystal 2d (nm)	Resolution (eV)
Al Kβ	1s ←OB	Al 3p	1545–65 eV	SiO$_2$ 1010 0.245 47	0.3
Fe Lα	2p$_{3/2}$ ←OB	Fe 3d–4s	700–10 eV	RbAP 2.6121	0.5

The surface of the Al–Fe samples were somewhat oxidized, so the spectra of Al or Fe in the oxides were obtained at the same time as the spectra of the elements in the alloys. Whereas there was a very faint oxide signal present on the Al spectra that could always be exactly removed from the raw data, we did not observe a significant oxide contribution to the Fe spectra except for A-Al$_{0.86}$Fe$_{0.14}$ (see next section).

The Al 2p$_{3/2}$ and Fe 2p$_{3/2}$ binding energies were measured with a Kratos spectrometer equipped with a Mg anode used in conditions such that the full width at half-maximum (FWHM) intensity of the Ag 3d$_{5/2}$ peak is 1 eV. The energy calibration was achieved by taking C 1s equal to 285.0 eV. The binding energy of the Al 1s level could not be obtained directly. It was determined owing to the complementary measurement of the energy of the x-ray transition Al 2p$_{3/2}$ → 1s. No difference was observed for this transition between the pure metal and the alloys. The experimental estimated error were ±0.1 eV for the Al 2p$_{3/2}$ level and ±0.3 eV for the Fe 2p$_{3/2}$ level; this is also the precision with which the Fermi level E_F has been set on the respective Al 3p and Fe 3d–4s x-ray transition energy scales.

2.4. Resistivity measurements

A classical four-point resistance measurement was performed on some samples while the temperature was varied from 4 to 300 K.

3. Results

3.1. Sample concentrations and structural states

The layered structure of the starting samples was clearly displayed by the Rutherford back-scattering spectra on the signal coming from both the Fe and the Al atoms, as seen in figure 1. The more intense peak located at 0.58 MeV is due to the superimposition of the signal coming from the first deposited Al layer and from the Si atoms in the substrate. The Rutherford back-scattering spectra of the irradiated samples demonstrates the effectiveness of the mixing mechanism as the peak structure has disappeared. The small signal located at high energy and of low amplitude comes from the presence of the Xe atoms used for the mixing. Some heterogeneities may be detected and quantitatively estimated with the fitting procedure (see table 1).
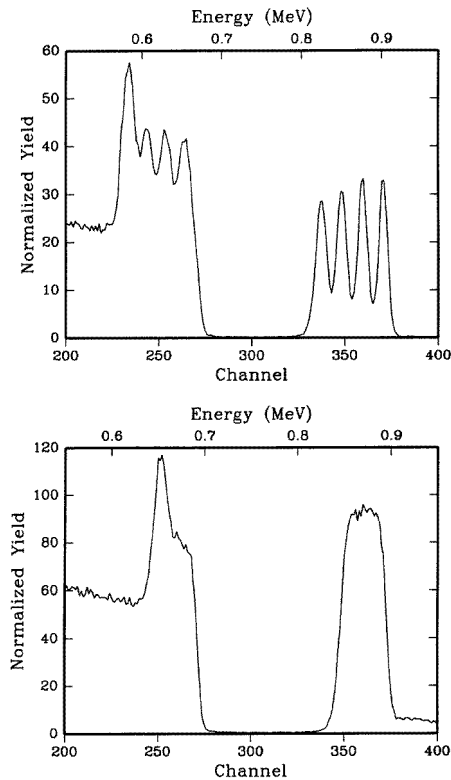

Figure 1. Rutherford back-scattering spectra of an unirradiated multilayer consisting of four Al/Fe bilayers (top) and of sample b (bottom).

The compositions quoted in table 1 are values averaged though the whole sample depth. In general it is necessary to involve some oxygen content in the sample surface in order to reproduce the experimental spectra well. This oxidation layer located at the sample surface attains 5–10% of the total sample thickness.

The Xe projected range R_p and width of the profile distribution were estimated by the simulation procedure. R_p is about 10–20% larger than calculated from the TRIM code (Ziegler *et al* 1986) whereas the width is in rather good agreement.

RBS also provides sample thicknesses of the order of 100 nm, and these values were used to calculate the resistivity of the samples from the resistance measurements.

Structural states identified by TEM are given in table 1 for the different sample treatments. The 190 °C irradiation temperature provides QC samples whereas room-temperature irradiation provides A samples.

3.2. Mössbauer spectroscopy

Typical Mössbauer spectra of A or QC states are presented on figure 2 together with the spectrum characteristic for the C-Al$_{15}$Fe$_2$ phase obtained from a sample after annealing treatment at 500 °C.
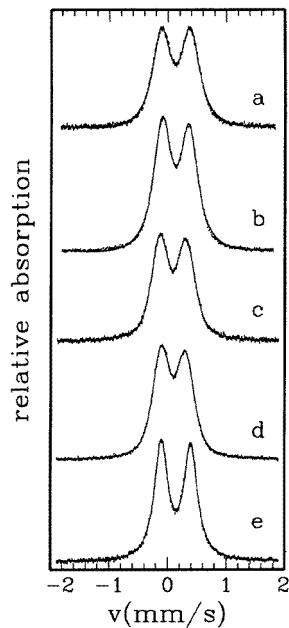

Figure 2. Experimental and fitted conversion electron Mössbauer spectra of as-irradiated multilayers according to table 1 (curves a–d) and sample a annealed at 500 °C (curve e).

In all cases the CEMS signal displays no traces of the magnetic sextet expected for α-Fe which is another indication of good mixing efficiency. A broadened quadrupole doublet is seen which was fitted as indicated above. The best fits were obtained with QSD, but representative values of QS and IS may also be obtained from the simpler fits of type (i).

In obtaining the QSDs from the spectra we determined its smoothness following the Hesse–Rubatsch criterion (Wivel and Morup 1981). The resulting QS distribution functions are nearly Gaussians without the features (two or more 'bumps') reported by Plenet *et al* (1993), which seem to be artefacts generated by the fitting procedure. Indeed, good fits of our spectra may also be obtained assuming a Gaussian distribution of Lorentzian doublets, i.e. a doublet of Voigt lines.

Fitted QSDs are displayed in figure 3 whereas the fitted parameters $\langle QS \rangle$, $\langle IS \rangle$, σ_{QS}, the spread of QS, and α are shown in table 3. Some general trends may be easily inferred from these values.
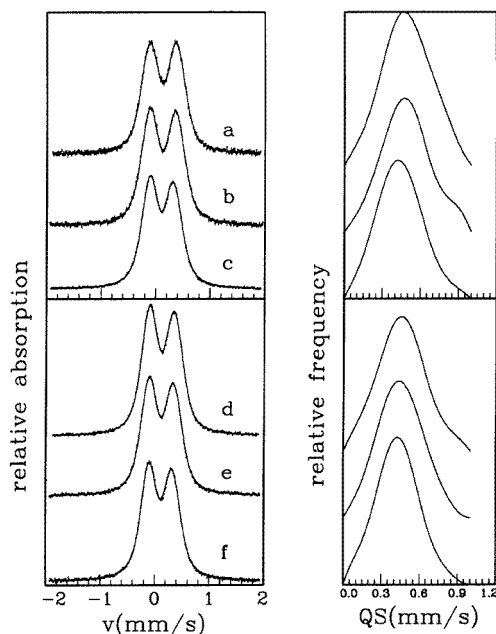
Figure 3. Experimental and fitted conversion electron Mössbauer spectra (left) and corresponding QS distribution (right): curves a–c, sample a as irradiated and after anneals at 200 °C and 350 °C, respectively; curves d–f, same for sample b.

Table 3. Fitted values from conversion electron Mössbauer spectra. Typical uncertainties are 0.001 mm s^{-1} in $\langle$QS$\rangle$, 0.002 mm s^{-1} in σ_{QS}, 0.003 mm s^{-1} in $\langle$IS$\rangle$ and 0.003 in α.

Sample	$\langle$QS$\rangle$ (mm s^{-1})	σ_{QS} (mm s^{-1})	$\langle$IS$\rangle$ (mm s^{-1})	α
a, as prepared	0.494	0.191	0.236	0.000
Annealed at 200 °C	0.488	0.190	0.233	0.020
Annealed at 350 °C	0.443	0.181	0.213	0.037
Annealed at 500 °C	0.501	0.000	0.254	($\Gamma = 0.279$)
b, as prepared	0.461	0.188	0.231	0.029
Annealed at 200 °C	0.454	0.179	0.221	0.038
Annealed at 350 °C	0.431	0.173	0.214	0.043
Annealed at 500 °C	0.505	0.000	0.253	($\Gamma = 0.291$)
c, as prepared	0.448	0.176	0.192	0.028
Annealed at 200 °C	0.439	0.173	0.186	0.048
d, as prepared	0.413	0.172	0.198	0.034
Annealed at 350 °C	0.390	0.165	0.192	0.036

(i) For a given composition, $\langle$IS$\rangle$ is almost independent of the structure, irradiation temperature and/or annealing treatment but depends strongly on the Fe content. Hence in figure 4 we have plotted our $\langle$IS$\rangle$ values together with those of other workers, whatever the sample structural state (Sawicka *et al* 1978, Dunlap *et al* 1988, Alexandre *et al* 1992,

Baumvol 1992, Plenet *et al* 1993). The value quoted from Dunlap *et al* (1988) is an average of the two reported IS values interpreted as coming from two different Fe sites. Except for one value from the work of Plenet *et al* (1993) which is slightly different, the ⟨IS⟩ all display the same tendency, i.e. an increase with increasing Fe content in the range $0 < x < 0.27$. This was already seen by Hsu and Chien (1991) for A or BCC random solid solutions.
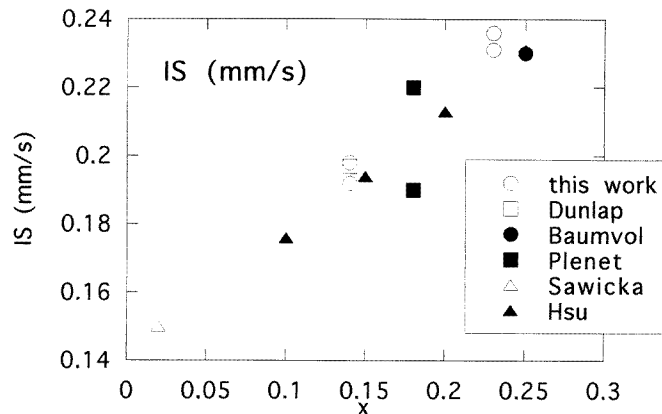

Figure 4. IS versus Fe content x: Dunlap, Dunlap *et al* (1988); Baumvol, Baumvol (1992); Plenet, Plenet *et al* (1993); Sawicka, Sawicka *et al* (1978); Hsu, Hsu and Chien (1991).

(ii) ⟨QS⟩ increases with increasing Fe concentration and for a given concentration it is considerably lower for samples irradiated at 190 °C (QC). On the other hand the spectra of these samples are more asymmetric than those of samples irradiated at 20 °C, as reflected by the fitted values of the IS–QS correlation parameter α.

Heat treatments at low temperatures (200 °C) produce minor variations, the main change being a ⟨QS⟩ reduction of about 0.01 mm s^{-1} in all cases whereas treatments at 350 °C produce important changes in the spectra; for samples b and d (mixed at 190 °C) the asymmetry increases and ⟨QS⟩ and σ_{QS} are considerably reduced. Furthermore, samples a (mixed at 20 °C) and b (mixed at 190 °C), when treated at 350 °C yield very similar mass spectra. Finally, the spectra of samples a and b, after treatment at 500 °C, are characteristic of the C-$A_{15}Fe_2$.

3.3. X-ray emission spectroscopy

Let us first recall the results for pure Al and Fe metals. The Al 3p emission curve displays a somewhat parabolic-like shape with an abrupt arctangent-like edge at E_F and an important tail towards high binding energies; due to this tail, the curve is normalized between the maximum and the intensity before the edge at about $E_F - 2$ eV. The emission edge crosses the Fermi level at half the maximum intensity; the maximum of the distribution curve is at about $E_F + 1.4$ eV and the FWHM is 5.2 ± 0.1 eV (table 4).

For Fe, due to transition probabilities, the Fe 3d–4s curve mainly reflects the 3d distribution. This curve is normalized between its maximum and the regions of the wings on each side of maximum where the variation in intensity is negligible. Its shape is almost symmetric; the summit is at $E_F + 2.3$ eV; the FWHM is 3.2 ± 0.1 eV. The Al 3p and Fe 3d–4s curves are shown in figure 5.

Table 4. From left to right, the first four columns display the energy of the maximum of the Al 3p distribution, the Al 3p intensity at E_F, the FWHM and the distance to E_F taken at half the maximum intensity. The last three columns give the energy of the maximum of the Fe 3d–4s distribution, the Fe 3d–4s intensity at E_F and the FWHM.

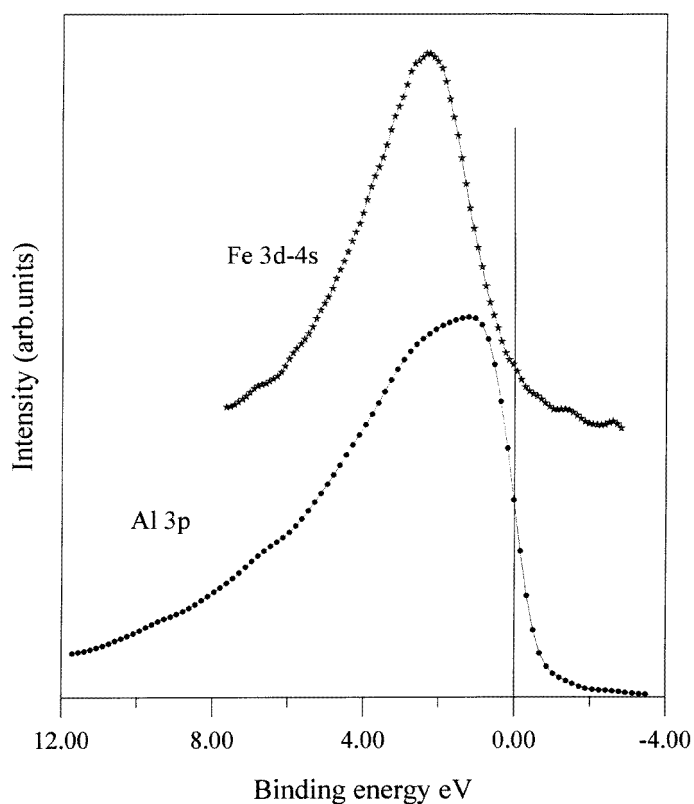| Sample	Al 3p maximum (eV)	I_{Al} ± 1	Al 3p FWHM (eV)	δ (eV)	Fe 3d maximum (eV)	I_{Fe} ± 2	Fe FWHM (eV)
Fe					2.3	17	3.2
Al	1.4	50	5.2	0			
$Al_{13}Fe_4$	2.4	17	4.4	0.6_5	1.0	63	3.2_5
$Al_{0.77}Fe_{0.23}$, annealed	2.5	19	4.4_5	0.6			
$Al_{0.77}Fe_{0.23}$, icosahedral	1.7	34	4.6_5	0.2	0.8_5	61	2.7
$Al_{0.86}Fe_{0.14}$, amorphous	1.9_5	32	4.7	0.3	0.8	56	3.0

Figure 5. Al 3p and Fe 3d–4s electronic distributions in the pure metals adjusted to the binding energy scale.

In figure 6 we show the same curves for icosahedral QC-$Al_{0.77}Fe_{0.23}$, A-$Al_{0.86}Fe_{0.14}$ and, for comparison, C-$Al_{13}Fe_4$. The Al 3p curve for annealed $Al_{0.77}Fe_{0.23}$ is also plotted in this figure. The normalization of the curves is the same as for the pure metals.

The Al 3p bands retain the same general shape from one sample to the other. However, at E_F the edge is less abrupt than for pure Al and it is slightly shifted towards the centre
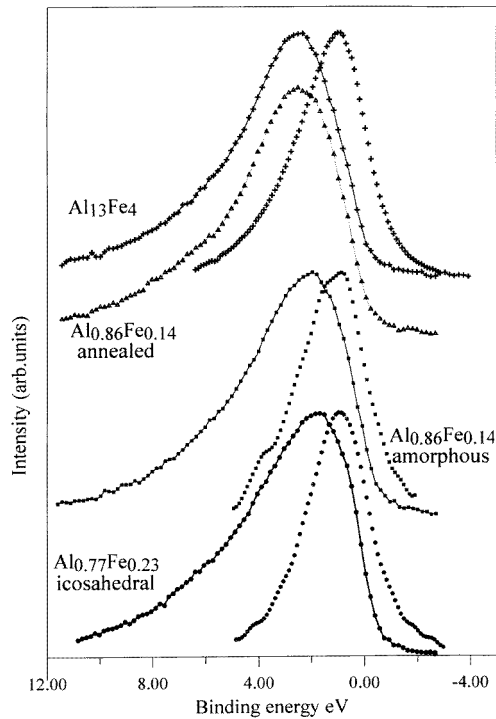
Figure 6. From bottom to top, Al 3p and Fe 3d–4s electronic distributions in icosahedral Al$_{0.77}$Fe$_{0.23}$ and A-Al$_{0.86}$Fe$_{0.14}$, Al 3p electronic distribution in annealed Al$_{0.86}$Fe$_{0.14}$ and Al 3p and Fe 3d–4s electronic distributions in C-Al$_{13}$Fe$_4$.

of the band; it shows two different slopes the change in which is seen by a marked step for C-Al$_{13}$Fe$_4$; whatever the sample, the rounded maximum is followed by a long tail whose intensity decreases monotonically against increasing binding energies. Table 4 gives the energies of the maxima of each curve, its FWHM, the intensity at E_F and the distance to E_F taken at half the maximum intensity of the band. We have reported above that the distance to the Fermi level is zero for pure Al. The fact that it differs from zero in the alloys indicates the formation of a pseudo-gap at E_F in the Al 3p distribution as already seen in QC- and A-(Al–Mn) phases (see Belin and Traverse (1991) and Berger *et al* (1993), and references therein). Note that the FWHM of the Al 3p distribution is narrower in the samples than in the pure metal, which we ascribe to the alloying with Fe that changes the Al local environment.

All the same, the shapes of the Fe 3d–4s curves are similar to that of pure Fe except, as already mentioned above, for the A-Al$_{0.86}$Fe$_{0.14}$ sample. For this alloy, a noticeable shoulder is seen about 4 eV from E_F as well as a slight broadening of the maximum; these are not noticeably observed for pure Fe nor for the other alloys; all this may be due to relevant oxidation of the sample. The various Fe 3d bands are narrower than for pure Fe which, as for Al, we ascribe to the changes in the local Fe environment in the alloys with respect to pure Fe. The values for the FWHM and the energy of the maxima of the Fe 3d bands are given in table 4.

The result of the Al–Fe alloying is to push the Al 3p bands towards the centre of the band with respect to pure Al whereas the Fe 3d bands are pushed closer to E_F than in the

pure metal. Consequently, at E_F, the Fe 3d intensity is higher in the alloys than in the pure Fe, whereas the Al 3p intensity is lower in the alloys than in pure Al. The corresponding values are shown in table 4. The Al 3p and Fe 3d states curves overlap in an energy range of about 3 eV from E_F; thus the states are mixed in this energy range. This suggests that the local environments may be about the same in the A and QC alloys.

3.4. Resistivity measurements

Values measured at 4 K are reported in table 5. They are plotted versus the Fe concentration in figure 7. Values from other workers are also shown for comparison. A smooth thermal dependence is observed in the investigated temperature range; as T increases, the resistivity first decreases, then increases and finally decreases again. However, the overall variations are only 0.5% and 10% for $x = 0.14$ and 0.23, respectively.

Table 5. Resistivity values versus concentration and structural states.

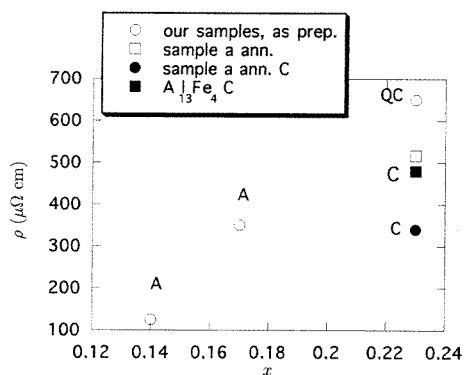| Sample	Resistivity at 4 K ($\mu\Omega$ cm)
$Al_{0.86}Fe_{0.14}$, amorphous	125
$Al_{0.83}Fe_{0.17}$, amorphous	351
$Al_{0.77}Fe_{0.23}$, icosahedral	650
$Al_{0.77}Fe_{0.23}$, annealed	340
$Al_{0.80}Mn_{0.20}$, decagonal (a)	420

Figure 7. Resistivity values versus the Fe concentration measured at 4 K for our samples and data from other workers.

4. Discussion

4.1. Phase formation in $Al_{1-x}Fe_x$ and ion beam mixing

Concerning the resulting structural states as a function of the irradiation temperature and Fe concentrations, we showed that A and QC single-phase $Al_{1-x}Fe_x$ can be prepared for $x = 0.14$ and $x = 0.23$. While the former concentration is the smallest reached to our knowledge by ion beam mixing, the latter, which lies in the range already studied, provides

a result in agreement with those of other workers (Baumvol 1992, Karpe *et al* 1992). Ion beam mixing turned out to be a better technique in this x range to prepare these compounds than thermal treatments. For example, a multilayered sample (Al and Fe layer thicknesses of 24 nm and 4 nm, respectively) with an average Fe concentration $x = 0.19$ formed a C-Al$_6$Fe phase after annealing at a temperature T between 250 and 450 °C (Csanady *et al* 1988). A mixture of QC phase and Al$_6$Fe was achieved for thinner layers (8 and 2 nm) (Csanady *et al* 1988).

An attempt to prepare by ion beam mixing a sample with $x = 0.12$ was not successful because of large in-depth inhomogeneities. According to our CEMS results, the majority of Fe atoms in this sample would be in regions with an Fe concentration higher than the average, yielding an IS value similar to those obtained in samples with $x = 0.14$. We must mention that by deposition at 300 °C a multilayered Al/Fe sample turns out to form a QC alloy (Csanady *et al* 1988).

We have mentioned the presence of small in-depth concentration inhomogeneities as seen by RBS of the order of 0.6–2.2%. In the work of Brenier *et al* (1994), inhomogeneities are revealed by SIMS measurements as well. However, they are of the order of 50% in the Fe concentration whereas the existence of C-Al$_5$Fe$_2$ and C-Al$_{13}$Fe$_4$ are detected by x-ray diffraction with an average concentration in the unirradiated system of $x = 0.17$. However, the experimental conditions are slightly different; the irradiation temperature is higher, 493 K, which might explain the crystal formation.

As mentioned, the $\langle$IS$\rangle$ is independent of the atomic structure for disordered phases (A, QC, C or random solid BCC solutions) and depends only upon composition. Although QS depends on the structure (QS$_{qc}$ < QS$_a$), the main difference between conversion electron Mössbauer spectra of A and QC phases of the same composition lies in the asymmetry reflected by the correlation parameter α. This is a rather empirical parameter that relates IS and QS linearly without any physical basis for this assumption. In this respect, it is worth noting that the parameter α also relates the spread of QS and IS values throughout the sample: $\sigma_{IS} = \alpha\sigma_{QS}$. It seems that σ_{IS}, rather than α, is the physical quantity to be considered in analysing the observed QSDs. Generally the increase in α accompanies a reduction in σ_{QS}, indicating that the reduction in σ_{IS} is not so large and, in some cases, is negligible. If we associate $\langle$IS$\rangle$ with the number and nature of Fe nearest neighbours we may conclude that, on the average, they are not much affected in going from A to QC phases, at least not so much as the topological order around Fe atoms is increased, as reflected by the reduction in QS and σ_{QS}.

4.2. Electronic properties versus Fe concentration

The occurrence of a pseudo-gap in Al$_{1-x}$Fe$_x$ is in agreement with previous observations from QC- and A-Al–Mn alloys (Belin and Traverse 1991). The resistivity increase versus the Fe concentration is thus correlated to a pseudo-gap formation.

For all the structural states studied, the $\langle$IS$\rangle$ depends mainly on concentration. The IS variation is related to the modification of the density of s electrons at the Fe site. When IS increases, the s electronic density decreases. In order to interpret the observed behaviour, it is interesting to look first at experimental observations in Al$_{1-x}$Fe$_x$ (0.27 < x < 1.00) alloys (Hsu and Chien 1991) where $\langle$IS$\rangle$ increases about 0.003 mm s^{-1} (% Al)$^{-1}$. According to these results as well as to theoretical predictions (Miedema and Van der Woude 1980), the primary effect on $\langle$IS$\rangle$ when introducing more and more Al atoms in an Fe-rich sample is a linear increase of its value due to a two-step process: firstly the charge transfer from Al to Fe and secondly the electronic redistribution in the Fe atomic shells. This interpretation is

done in the framework of a rigid-band model where the Fe electron distribution is not very much perturbed by Al alloying.

In the range of Fe contents studied here, our values plus others quoted in figure 4 indicate a drastic change in the $\langle IS \rangle$ behaviour since here $\langle IS \rangle$ increases about 1.5 mm s^{-1} (% Fe)$^{-1}$. The rigid-band model is thus no longer valid. SXES might give information on this point. We did not measure the Fe electronic distribution in an Fe-rich Al–Fe alloy. However, we can reasonably presume that the Fe 3d states are not very different from those measured in pure Fe (figure 5). On the other hand, in the Al-rich alloys the Fe 3d states are modified. They are pushed upwards closer to the Fermi level whereas the Al 3p states are pushed down towards the bottom of the band. There is less overlapping of the occupied Fe d and Al p states. Now we shall assume that, in addition to what is experimentally observed, there is dehybridization of the Fe d and s states, the Fe s states being pushed down to the bottom of the band overlapping with the p states of Al. In such a situation, there is a spreading of the Fe d and s electronic states. Hence the first step mentioned to explain the $\langle IS \rangle$ variation is still valid whereas the second step, the electron redistribution inside the Fe states, might be more difficult to achieve. There is thus an increase in s electronic character at the Fe site given by Al when the Al content increases, which leads to the observed $\langle IS \rangle$ behaviour.

5. Conclusion

Two $Al_{1-x}Fe_x$ systems with $x = 0.14$ and $x = 0.23$, were prepared in the A and QC structural states by ion beam mixing. A C state was obtained by subsequent thermal treatments. The evolution of the following electronic properties was analysed versus the Fe content and the structural states: the IS in Mössbauer spectroscopy, the electronic distributions of the p electrons of Al and d electrons of Fe, and the electrical resistivity. The last parameter which is more sensitive to the long-range atom order is lower in the C state than in the A and QC states for the same x-value. The average resistivity increase with increasing Fe content is explained by the Al intensity decrease at the Fermi level due to the occurrence of a pseudo-gap in the Al 3p electronic distribution as observed from SXES. The IS evolution is interpreted in terms of the electronic rehybridization of the p electrons of Al and d electrons of Fe but also in terms of dehybridization of the s and d electrons of Fe.

References

Alexandre J L, Vasconcellos M A Z, Hübler R, Texeira S R and Baumvol I J R 1992 *Nucl. Instrum. Methods* B **80–1** 436
Baumvol I J R 1992 *Nucl. Instrum. Methods* B **80-1** 363
Belin E and Traverse A 1991 *J. Phys.: Condens. Matter* **3** 2157
Berger C, Belin E and Mayou D 1993 *Ann. Chim. Fr.* **18** 485, and references therein
Bernas H *et al* 1992 *Nucl. Instrum. Methods* B **62** 416
Brenier R, Canut B, Gea L, Ramos S M M, Thevenard P, Dubois C, Dupuy J C, Prudon G and Brunel M 1994 *J. Physique IV Coll.* **4** C3 263

Csanady A, Günter J R, Barna P B and Mayer J 1988 *Thin Solid Films* **167** 203

Doolittle L R 1986 *Nucl. Instrum. Methods* B **15** 227

Dunlap R A, Lawther D W and Lloyd D J 1988 *Phys. Rev.* B **38** 3649

Hohmuth K, Heera V and Rauschenbach B 1989 *Nucl. Instrum. Methods* B **39** 136

Hsu J H and Chien C L 1991 *Hyperfine Interact.* **69** 454

Karpe K, Kyllesbech Larsen K and Bøttiger J 1992 *Phys. Rev.* B **46** 2686

Miedema A R and Van der Woude F 1980 *Physica* B **100** 145

Pierce F S, Poon S J and Guo Q 1993 *Science* **261** 737, and references therein

Plenet J C, Perez A, Rivory J and Laborde O 1993 *Phys. Rev.* B **47** 3021

Poon S J, Pierce F S, Guo Q and Volkov P 1995 *Proc. 5th Int. Conf. on Quasicrystals* ed C Janot and R Mosseri
    (Singapore: World Scientific) at press, and references therein

Sawicka B D, Drwiega M, Sawicki J and Stanek J 1978 *Hyperfine Interact.* **5** 147

Shechtman D, Blech I, Gratias D and Cahn J W 1984 *Phys. Rev. Lett.* **53** 1951

Tsai A P, Inoue A and Masumoto T 1988 *Japan. J. Appl. Phys.* **27** L1587

Wivel C and Morup S 1981 *J. Phys. E: Sci. Instrum.* **14** 605

Ziegler J F, Biersack J P and Littmark U 1986 *The Stopping and Range of Ions in Solids* (Oxford: Pergamon)